

Hamburger Beiträge

zur Angewandten Mathematik

A Limiter-Based Well-Balanced Discontinuous Galerkin Method for Shallow-Water Flows with Wetting and Drying: One-Dimensional Case

Stefan Vater, Nicole Beisiegel, Jörn Behrens

Nr. 2015-12
March 2015

A Limiter-Based Well-Balanced Discontinuous Galerkin Method for Shallow-Water Flows with Wetting and Drying: One-Dimensional Case

Stefan Vater^{a,*}, Nicole Beisiegel^a, Jörn Behrens^{b,a}

^a*CEN – Center for Earth System Research and Sustainability, Universität Hamburg, Grindelberg 5, 20144 Hamburg, Germany*

^b*Department of Mathematics, Universität Hamburg, Bundesstraße 55, 20146 Hamburg, Germany*

Abstract

An important part in the numerical simulation of tsunami and storm surge events is the accurate modelling of flooding and the appearance of dry areas when the water recedes. This paper proposes a new algorithm to model inundation events with piecewise linear Runge-Kutta discontinuous Galerkin approximations applied to the shallow water equations. This study is restricted to the one-dimensional case and shows a detailed analysis and the corresponding numerical treatment of the inundation problem.

The main feature is a velocity based “limiting” of the momentum distribution in each cell, which prevents instabilities in case of wetting or drying situations. Additional limiting of the fluid depth ensures its positivity while preserving local mass conservation. A special flux modification in cells located at the wet/dry interface leads to a well-balanced method, which maintains the steady state at rest. The discontinuous Galerkin scheme is formulated in a nodal form using a Lagrange basis. The proposed wetting and drying treatment is verified with several numerical simulations. These test cases demonstrate the well-balancing property of the method and its stability in case of rapid transition of the wet/dry interface. We also verify the conservation of mass and investigate the convergence characteristics of the scheme.

Keywords: Shallow water equations, Discontinuous Galerkin, Wetting and Drying, Limiter, Well-balanced Scheme

1. Introduction

The shallow water equations are an established model for geoscientific applications such as tsunami or storm surge simulations [see e.g. 4, 21]. Although they are derived under the assumption that vertical velocities are negligible,

*stefan.vater@uni-hamburg.de

they are favored for their ability to realistically model large scale horizontal flows with relatively low computational cost. While the discrete representation of the flow field and the propagation of surface waves in the deep ocean is usually well captured, difficulties arise in the coastal area, where water floods originally dry areas or recedes back into the ocean. Mathematically, this is a problem, because the shallow water equations become ill-posed when the fluid depth becomes zero. Therefore, either the computational domain must be dynamically adapted according to the edge of the water body, or one needs to introduce a special treatment of wetting and drying events into the numerical scheme.

Although the Lagrangian approach of a moving mesh is known to result in accurate solutions, its implementation is difficult, especially in case of complex bathymetry, and only applications to simple flow configurations have been reported in the literature [3, 17]. Thus, in geophysical problems it turned out to be advantageous to use meshes which do not necessarily align with the wet/dry interface. In this Eulerian approach one has to ensure the positivity of the fluid depth, the proper treatment of dry cells and the discrete representation of steady states (well-balancing). Furthermore, the scheme must stably deal with a possibly ill-conditioned velocity near the wet/dry interface when computations are carried out with fluid depth and momentum as primary variables and the velocity is computed as quotient of both quantities. This is especially the case in Godunov-type schemes, which employ the use of Riemann solvers for the flux computation at discontinuous interfaces in the discrete solution.

There have been various approaches to deal with wetting and drying, most of them using finite volume discretization techniques. In this area, the work of Audusse et al. [1] introduced a general treatment of inundation modeling. Their principle of hydrostatic reconstruction together with a well-balanced discretization of the source term has become widely used and further developed [see e.g. 16, 18, 26]. Although finite volume methods have demonstrated their robustness and can perfectly conserve mass, they also have their shortcomings. Most notably, they only provide cell mean values as solution components and the computation of higher order approximations involves an increasing stencil of cells [14, 20], which becomes complicated for unstructured grids. On the other hand, continuous finite element methods provide pointwise solutions, and they can relatively easily be extended to higher order by using higher order shape functions. The problem in using finite element methods for advection dominated problems is the continuity condition on the solution, which renders most methods unconditionally unstable, and they must be stabilized by adding artificial viscosity.

In this context, discontinuous Galerkin (DG) methods are a good compromise. They borrow the conservation property from finite volume methods by using local shape functions which are discontinuous across cell interfaces. Communication between cells is modeled by fluxes as in finite volume methods. Higher-order accuracy can be achieved by using high-order shape functions. Compared to continuous finite elements of the same order, discontinuous Galerkin methods need a higher number of degrees of freedom and have a strict time step restriction, but the locality of their shape functions simplifies adaptivity and the parallelization of the method.

Modeling wetting and drying in shallow water flows using discontinuous Galerkin methods is still a very young research area and mostly restricted to linear elements. Bokhove [5] applied a moving mesh approach with free boundary elements at the wet/dry interface, while other approaches were based on fixed meshes. A nodal flux modification technique was introduced by Gourgue et al. [12]. The most common approach is based on slope-limiting. Kesserwani & Liang [15] directly adapted the idea of hydrostatic reconstruction to a Runge-Kutta discontinuous Galerkin (RKDG) discretization. The works in [6, 9, 27] introduced a scaling around the mean within each cell to obtain positivity of the fluid depth as well as mass conservation. Most of these studies concentrated on the positivity of the fluid depth and the well-balancing property, so far. The ill-conditioned computation of the velocity has only been implicitly dealt with by using restrictive limiters, such as the corrected Minmod-limiter in [27], or, as in [9] by setting an upper problem dependent tolerance of the velocity.

The problem of stably computing the velocity is addressed in this study in the context of a limiter based treatment of inundation events. The basic idea is that the momentum variable is modified on the basis of the resulting velocity distribution given a fixed (but already limited) distribution of the fluid depth. This results in a stable flux computation which usually involves the computation of the velocity at some point. The general idea is borrowed from finite volume methods, where limiting in other than the primary flow variables often enhances the solution. However, in finite volume methods, these limited values are only used for the flux computation at the cell interfaces. In discontinuous Galerkin methods, on the other hand, the solution itself is limited and further used throughout the computations. Therefore, the non-trivial in-cell functional behavior of the velocity, which is the quotient of two polynomials, cannot be ignored in the limiting process. To the authors' knowledge this concept of limiting in other than the primary variables has not been thoroughly transferred to discontinuous Galerkin methods, yet.

In addition, the proposed method is fully mass conservative and well-balanced in that it preserves the steady state at rest. Here, we restrict ourselves to the one-dimensional case to introduce the basic principles and to better analyze the details of the algorithm. The extension of the scheme to two space dimensions will be left to a sequel study. Starting from the governing equations, the Runge-Kutta discontinuous Galerkin method is introduced in the next section. On this basis, a detailed description of the new wetting and drying treatment is given in section 3, which is verified in several test cases in section 4. The paper closes with a final discussion and conclusions in section 5.

2. The shallow water equations and their RKDG discretization

The one-dimensional shallow water model is defined by two equations, the first stating the conservation of mass and the second describing the balance of forces in form of the momentum equation. The system can be written in the

compact conservative form

$$\mathbf{U}_t + \mathbf{F}(\mathbf{U})_x = \mathbf{S}(\mathbf{U}) \quad (1)$$

where the vector of unknowns is given by $\mathbf{U} = (h, hu)^\top$. Here and below, we have written the partial derivatives with respect to time t and space x as indices, i.e., $\mathbf{U}_t \equiv \frac{\partial \mathbf{U}}{\partial t}$. The quantity $h = h(x, t)$ denotes the fluid depth of a uniform density water layer and $u = u(x, t)$ is the depth-averaged horizontal particle velocity. The flux function is defined by $\mathbf{F}(\mathbf{U}) = (hu, hu^2 + \frac{g}{2}h^2)^\top$, where g is the gravitational constant. Furthermore, the bathymetry (bottom topography) $b = b(x)$ is represented by the source term $\mathbf{S}(\mathbf{U}) = (0, -ghb_x)^\top$.

For the discretization the governing equations are solved on the domain $[x_{\min}, x_{\max}]$, which is divided into intervals (cells) $I_i = (x_{i-1/2}, x_{i+1/2})$. On each interval, the equations (1) are multiplied by a test function φ and integrated. Integration by parts of the flux term leads to the weak DG formulation

$$\int_{I_i} \mathbf{U}_t \varphi \, dx - \int_{I_i} \varphi_x \mathbf{F}(\mathbf{U}) \, dx + \left[\mathbf{F}^*(\mathbf{U}) \varphi \right]_{x_{i-1/2}}^{x_{i+1/2}} = \int_{I_i} \mathbf{S}(\mathbf{U}) \varphi \, dx. \quad (2)$$

Note that the interface flux \mathbf{F}^* is not defined in general, since the solution can have different values at the interface in the adjacent cells. This problem is circumvented in the discretization by using the (approximate) solution of the corresponding Riemann problem. For the simulations in this study we used the Rusanov solver [24], but other Riemann solvers such as HLLE [8] gave similar results.

System (2) is further discretized using a semi-discretization in space with a piecewise polynomial ansatz for the discrete solution components and test functions φ_k . To obtain second-order accuracy, we use piecewise linear functions, which are represented by nodal Lagrange basis functions [10, 13]. In view of a two-dimensional extension of the scheme, n -point Gauß-Legendre quadrature is applied to obtain an (exact) discretization of the integral terms. In each cell, this discretization in space leads to a system of ordinary differential equations (ODEs) for the vector of degrees of freedom $\tilde{\mathbf{U}}_i(t)$, where $\mathbf{U}(x, t) = \sum_j (\tilde{\mathbf{U}}_i)_j \varphi_j$ for $x \in I_i$. It is of the form

$$\frac{\partial \tilde{\mathbf{U}}_i}{\partial t} = \int_{I_i} \left(\hat{\varphi}_x \mathbf{F}(\mathbf{U}) + \hat{\varphi} \mathbf{S}(\mathbf{U}) \right) dx - \left[\hat{\varphi} \mathbf{F}^*(\mathbf{U}) \right]_{x_{i-1/2}}^{x_{i+1/2}} =: \mathbf{H}_h(\tilde{\mathbf{U}}_i), \quad (3)$$

where $\hat{\varphi} = \mathbf{M}^{-1}(\varphi_k)_k$ and \mathbf{M} is the local mass matrix with $\mathbf{M}_{jk} = \int_{I_i} \varphi_j \cdot \varphi_k \, dx$. The resulting system for the degrees of freedom of all cells $\tilde{\mathbf{U}}_h$ is then solved using a total-variation diminishing (TVD) s -stage Runge-Kutta scheme [11, 19], which is of the general form

$$\begin{aligned} \tilde{\mathbf{U}}_h^{(0)} &= \tilde{\mathbf{U}}_h^n \\ \tilde{\mathbf{U}}_h^{(p)} &= \Pi_h \left\{ \sum_{q=0}^{p-1} \alpha_{pq} \tilde{\mathbf{U}}_h^{(q)} + \beta_{pq} \Delta t^n \mathbf{H}_h(\tilde{\mathbf{U}}_h^{(q)}) \right\} \quad \text{for } p = 1 \dots s \\ \tilde{\mathbf{U}}_h^{n+1} &= \tilde{\mathbf{U}}_h^{(s)} \end{aligned}$$

with Runge-Kutta coefficients α_{pq} and β_{pq} and a time step size $\Delta t^n = t^{n+1} - t^n$. $\mathbf{H}_h(\tilde{\mathbf{U}}_h)$ represents the right hand side of the ODE (3) extended to all cells. The limiter Π_h , which is applied in each Runge-Kutta stage p to an intermediate solution $\mathbf{U}_h^{(p)}$, is usually employed to stabilize the scheme in case of discontinuities. However, as stated above it can be also used for dealing with the problem of wetting and drying. In the remainder of this article, we use Heun’s method, which is the second-order representative of a standard Runge-Kutta TVD scheme. This completes the description of the Runge-Kutta discontinuous Galerkin (RKDG) method.

For (2), exact quadrature rules are a basic requirement for well-balancing [25]. At the cell interfaces no problems occur, since we use a continuous representation for the bottom topography. Otherwise, one can use the technique introduced in [25, 27], which is based on hydrostatic reconstruction of the interface values [1] and adds a higher order correction to the source term.

3. Wetting and drying algorithm

When it comes to wetting and drying, i.e. parts of the domain have water depth $h = 0$, several problems arise which must be handled by the numerical algorithm. First, the wet-dry transition might be within a cell and cannot be exactly represented by a piecewise (smooth) polynomial DG discretization (cf. Figure 1). The result is the occurrence of artificial gradients in the surface elevation that can influence the tendencies of the momentum equation and render the scheme unbalanced. Furthermore, one must ensure that the fluid depth remains non-negative. Otherwise the shallow water equations are undefined at these points. The third and in the authors’ opinion least investigated problem is that near the wet/dry interface, both, fluid depth and momentum go to zero, which yields an ill-conditioned computation of the velocity $u = (hu)/h$ in these regions.

In the following, it is first described how to deal with the occurrence of artificial gradients at the wet/dry interface. After that a new limiter is introduced, which prevents the fluid depth from being negative and controls the ill-conditioned computation of the velocity through the limitation of the momentum variable.

3.1. The wet/dry interface

Depending on the flow configuration a DG discretization might be more or less of physical nature near the wet/dry interface. According to Bates & Hervouet [3] (see also [6]) we distinguish between two general situations, which will be referred to as of “flooding”-type and “dam-break”-type (Figure 1). In the flooding-type situation the water comes from the deep water and the water level might successively rise. This situation also includes the still water lake at rest, where nothing happens. This can lead to unphysical gradients of the surface elevation as can be seen in the left part of Figure 1. In the “dam-break”

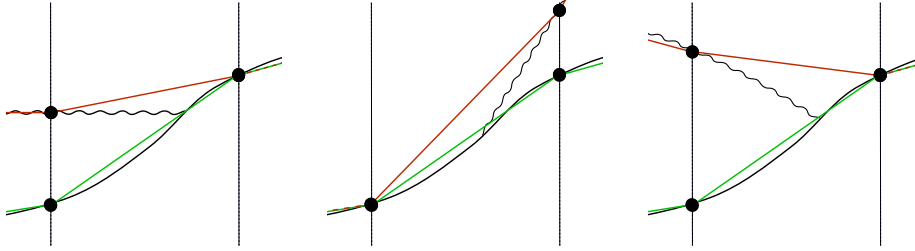


Figure 1: Discretization of different semi-dry cell types using the discontinuous Galerkin scheme with piecewise linear elements (red: surface elevation, green: bottom topography). Displayed are flooding-type (left) and two different dam-break-type (middle and right) cells. Note the artificial gradient in surface elevation introduced by the discretization in the flooding-type situation.

situation the water comes from above, like in the event of an upstream dam-break. There are two different configurations which are displayed in the middle and on the right of Figure 1 and considered to be discretized physically correct.

Therefore, we only modify the computation of the momentum tendencies in the flooding-type situation. Such cells can be identified by comparing the maximum value of the surface elevation $H = h + b$ with the maximum in bottom topography b within each cell, i.e., for cell I_i we check if

$$\max_{x \in I_i} H(x) - \max_{x \in I_i} b(x) < \text{TOL}_{\text{wet}} ,$$

where TOL_{wet} is a tolerance for the water depth under which it is considered dry. Since in the given piecewise linear configuration the extreme values are attained in the two vertices (Lagrange nodes) of a cell, it suffices to check the condition in these two points.

In the flooding-type cells the inner flux and source terms due to gravitational forces are neglected, which is equivalent to setting g equal to zero in these terms. The interface flux at the dry node is zero due to zero fluid depth. However, the flux term at the wet interface has to be considered, since it is also present for the adjacent wet cell. In order to be well-balanced in the semi-dry cell, we add a flux term including only the gravitational part computed on the basis of the fluid depth from the semi-dry cell at the wet interface. For a configuration as in Figure 1 (left) – assuming that this is cell I_i – the momentum equation in this cell then reads

$$\int_{I_i} (hu)_t \varphi \, dx - \int_{I_i} \varphi_x hu^2 + \frac{g}{2} h^2 \varphi \, dx + \left[(F_{hu}^* \varphi)(x_{i+1/2}) - (F_{hu}^* \varphi)(x_{i-1/2}) \right] + \frac{g}{2} (h^2 \varphi)(x_{i-1/2,+}) = 0 ,$$

where $(h^2 \varphi)(x_{i-1/2,+})$ is the value of $h^2 \varphi$ at $x_{i-1/2}$ based on the function values from cell I_i . Since $(F_{hu}^* \varphi)(x_{i-1/2}) = \frac{g}{2} (h^2 \varphi)(x_{i-1/2,+})$ and $u \equiv 0$ in the still water steady state this ensures that all flux terms vanish and the momentum tendency is zero.

3.2. Velocity based “limiting” of momentum

While limiting was originally introduced to obtain stable computations involving shocks, here we employ this numerical technique to stably discretize the wet/dry interface. Since the limiting modifies the solution itself in a DG method, and not only the values for the computation of the interface fluxes as in finite volume methods, further care must be taken for well-balancing. Therefore, we require that the limiter does not alter the steady state of the lake at rest. This is ensured by the Barth-Jespersen limiter [2] with limiting in hydrostatic variables, i.e., in $H = h + b$, which will be used throughout this work. This limiter essentially limits the in-cell distribution such that it does not exceed the minimum and maximum cell mean values of the surrounding cells. As we will see in the test cases, numerical evidence shows that limiting in fluid depth h improves the drying process at the coast in some situations considerably. As an alternative we propose a blending between the two limiting procedures in H and in h to balance the different requirements for the scheme.

Concerning the positivity of the fluid depth, Xing et al. [27] have shown that a fluid depth, which is initially positive in certain quadrature points, leads to positive mean values provided a suitable CFL condition is met. For piecewise linear polynomials the quadrature points of the trapezoidal rule are relevant. These are the nodal values in each cell. The resulting CFL condition to ensure positivity in the mean is $c_{\max}\Delta t/\Delta x \leq 1/2$, where $c_{\max} = \max\{|u| + \sqrt{gh}\}$. This condition is less restrictive than the CFL condition for linear stability of the DG method, the latter being $c_{\max}\Delta t/\Delta x \leq 1/3$ for piecewise linear polynomials. Positivity of the whole distribution is then obtained by scaling around the cell mean values. Further details can be found in [27].

The linear momentum distribution is “limited” by analyzing the resulting velocity distribution. This provides a stable computation near the wet/dry interface in the situation when both, h and (hu) get small. As we will see, the modified momentum can have a higher in-cell variation in some cases.

We start the description of the limiter by specifying the limiting process in $H = h + b$ (resp. h) on a nodal basis. Let $H_{i-1/2,+} = H_i(x_{i-1/2})$ and $H_{i+1/2,-} = H_i(x_{i+1/2})$ be the nodal values based on the linear distribution within cell I_i , and define the cell mean value and variation by

$$\bar{H}_i = \frac{H_{i+1/2,-} + H_{i-1/2,+}}{2} \quad \text{and} \quad \Delta H_i = \frac{H_{i+1/2,-} - H_{i-1/2,+}}{2} .$$

Then in a nodal based form the limiting in H can be computed from a limited in-cell variation, which is given by

$$\Delta H_i^{\text{lim}} = \text{sign}(\Delta H_i) \cdot \min\{|\Delta H_i|, |\bar{H}_{i+1} - \bar{H}_i|, |\bar{H}_i - \bar{H}_{i-1}|\} .$$

The limited nodal values are

$$\begin{aligned} H_{i-1/2,+}^{\text{lim}} &= H_{i-1/2,+} + (\Delta H_i - \Delta H_i^{\text{lim}}) \quad \text{and} \\ H_{i+1/2,-}^{\text{lim}} &= H_{i+1/2,-} + (\Delta H_i^{\text{lim}} - \Delta H_i) . \end{aligned}$$

The limited values for the fluid depth are obtained from $h_{i\pm 1/2,\mp}^{\text{lim,final}} = H_{i\pm 1/2,\mp}^{\text{lim}} - b_{i\pm 1/2,\mp}$.

This procedure can be applied in the same way to h , resulting in different, unbalanced in-cell distributions, but it can improve the drying process as stated above. Therefore, we introduce an alternative limiting procedure. Since both results from either limiting in H or h are linear and preserve the mean state, any convex linear combination does so, as well. We define a blending parameter, which linearly varies between 0 and 1 for minimum in-cell surface elevations H_{\min} between the minimum and maximum in-cell bathymetry values b_{\min} and b_{\max} . It is given by

$$\lambda = \max\left(0, \min\left(1, \frac{H_{\min} - b_{\min}}{b_{\max} - b_{\min}}\right)\right)$$

and the final nodal values are computed by

$$h_{i\pm 1/2,\mp}^{\text{lim,final}} = \lambda(H_{i\pm 1/2,\mp}^{\text{lim}} - b_{i\pm 1/2,\mp}) + (1 - \lambda)h_{i\pm 1/2,\mp}^{\text{lim}}.$$

For the velocity based ‘‘limiting’’ of the momentum variable let $u_i = (\overline{hu})_i/\overline{h}_i = (hu)_i(x_i)/h_i(x_i)$ be the velocity resulting from the mean values and $u_{i\pm 1/2,\mp} = (hu)_i(x_{i\pm 1/2})/h_i(x_{i\pm 1/2})$ the velocities in the vertices based on the distributions of cell I_i . Then the minimum and maximum velocities computed from the mean values of the surrounding cells are denoted by

$$u_i^{\min} = \min\{u_{i-1}, u_i, u_{i+1}\} \quad \text{and} \quad u_i^{\max} = \max\{u_{i-1}, u_i, u_{i+1}\}.$$

Each vertex value is limited to be within the bounds of u_i^{\min} and u_i^{\max}

$$\begin{aligned} u_{i-1/2,+}^{\text{lim}-} &= \max\{\min\{u_{i-1/2,+}, u_i^{\max}\}, u_i^{\min}\} \\ u_{i+1/2,-}^{\text{lim}+} &= \max\{\min\{u_{i+1/2,-}, u_i^{\max}\}, u_i^{\min}\} \end{aligned}$$

and the resulting velocity in the respective other vertex is computed by assuming a linear momentum distribution with prescribed mean value and a (fixed) linear distribution of the fluid depth:

$$\begin{aligned} u_{i+1/2,-}^{\text{lim}-} &= \frac{(\overline{hu})_i + ((\overline{hu})_i - h_{i-1/2,+}^{\text{lim}} \cdot u_{i-1/2,+}^{\text{lim}-})}{h_{i+1/2,-}^{\text{lim}}} \\ u_{i-1/2,+}^{\text{lim}+} &= \frac{(\overline{hu})_i - (h_{i+1/2,-}^{\text{lim}} \cdot u_{i+1/2,-}^{\text{lim}+} - (\overline{hu})_i)}{h_{i-1/2,+}^{\text{lim}}} \end{aligned}$$

Finally, the momentum distribution with the smallest in-cell velocity variation is chosen. We set

$$\Delta m_i^{\text{lim}} = \begin{cases} u_{i+1/2,-}^{\text{lim}+} \cdot h_{i+1/2,-}^{\text{lim}} - (\overline{hu})_i & \text{if } \left| u_{i+1/2,-}^{\text{lim}+} - u_{i-1/2,+}^{\text{lim}+} \right| < \\ & \left| u_{i+1/2,-}^{\text{lim}-} - u_{i-1/2,+}^{\text{lim}-} \right| \\ (\overline{hu})_i - u_{i-1/2,+}^{\text{lim}-} \cdot h_{i-1/2,+}^{\text{lim}} & \text{otherwise} \end{cases}$$

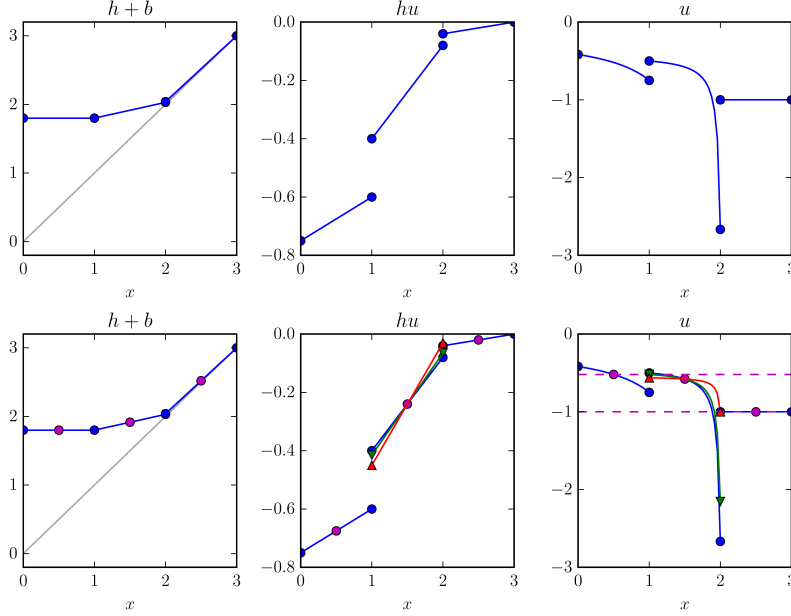


Figure 2: Visualization of the velocity based “limiting” of the momentum. Initial distribution in surface elevation, momentum and velocity (top row) and limiting procedure (bottom row).

and compute the nodal values of the momentum by

$$\begin{aligned} (hu)_{i-1/2,+}^{\text{lim}} &= (hu)_{i-1/2,+} + (\Delta m_i - \Delta m_i^{\text{lim}}), \\ (hu)_{i+1/2,-}^{\text{lim}} &= (hu)_{i+1/2,-} + (\Delta m_i^{\text{lim}} - \Delta m_i), \end{aligned}$$

where $\Delta m_i = (hu)_{i+1/2,-} - (\overline{hu})_i$. For further stabilization we set the momentum to zero in all nodes where the fluid depth drops under the wet tolerance:

$$(hu)_{i\pm 1/2,\mp}^{\text{lim,final}} = \begin{cases} 0 & \text{if } h_{i\pm 1/2,\mp}^{\text{lim}} < \text{TOL}_{\text{wet}} \\ (hu)_{i\pm 1/2,\mp}^{\text{lim}} & \text{otherwise.} \end{cases}$$

To illustrate the velocity based limiting it is visualized in Figure 2, where we have compiled a possible configuration in surface elevation and momentum at the wet/dry interface in the top row. The resulting velocity distribution is displayed in the rightmost figure. As one can see, the velocity in the center cell has an unphysical extreme value at $x = 2$, where both, fluid depth and momentum become small. For the limiting, the cell mean values of h and (hu) are computed and upper and lower limits for the velocity are derived (dashed magenta line). This results in two limited velocity and associated momentum distributions, which are marked as red and green with triangles at the end points. The final distribution is the velocity distribution with the smallest in-cell variation – in this case it is the red one. As one can see the associated

momentum distribution has a slightly bigger in-cell variation compared to the original one.

4. Numerical results

In this section the presented numerical scheme is tested against different configurations with wet/dry interfaces. Some address the well-balancing property of the method such as the classical “lake at rest”, others elaborate on the stability such as the oscillatory flow in a parabolic basin. A more realistic situation is simulated by a long-wave runup onto a beach, which resembles the arrival of a tsunami at the coast. In all simulations the gravitational constant is set to $g = 9.81$. Here and below we omit the dimensions of the physical quantities, which should be thought in the standard SI system with m (meter), s (seconds) etc. as basic units. The discrete initial conditions and the bottom topography are derived from the analytical ones by interpolation at the nodal (cell interface) points. The wet tolerance is set to $\text{TOL}_{\text{wet}} = 10^{-8}$, and we use limiting in $H = h + b$ if not stated otherwise. As stated above, a CFL number $\text{cfl} \leq 1/3$ results in a time step $\Delta t = \text{cfl}\Delta x/c_{\text{max}}$ which provides a stable and positive solution. In the following simulations, we always choose a fixed time step which satisfies this stability constraint. Besides fluid depth and momentum we also often show the velocity, which is derived by the quotient of the two other quantities.

4.1. Lake at rest

To verify the well-balancing property of the scheme, a basin is setup with a fluid at rest and an initially horizontal surface elevation. The test domain $[0, 1]$ has periodic boundary conditions. In the middle of the domain is an island, which is defined by the bottom topography

$$b(x) = \tilde{b}(r) = \begin{cases} a \cdot \frac{\exp(-0.5/(r_m^2 - r^2))}{\exp(-0.5/r_m^2)} & \text{if } r < r_m, \\ 0 & \text{otherwise} \end{cases}$$

where $r = |x - 0.5|$, and the parameters are set to $a = 1.2$ and $r_m = 0.4$. The initial fluid depth is $h(x, 0) = \min(0, 1 - b(x))$ (see Figure 3). The initial momentum is set to $(hu)(x, 0) \equiv 0$, which means that the fluid is in steady state. The domain is discretized into 50 cells, and the timestep is set to 0.002. This corresponds to a CFL number of 0.3. The solution is integrated over 10 000 timesteps until $t_{\text{max}} = 20$.

As in case of the exact solution, the discrete initial conditions should be preserved and only small deviations due to numerical truncation errors should occur. In Figure 4 the errors in fluid depth and momentum are displayed over time using the maximum norm. It can be seen that for both variables only errors within the range of machine accuracy develop.

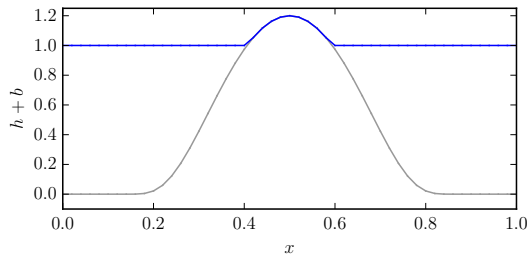


Figure 3: Initial surface elevation for the “lake at rest” test case. Depicted are the bathymetry (grey) and total water depth (blue).

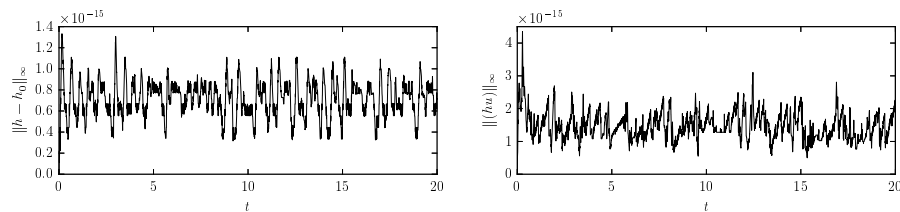


Figure 4: Errors in fluid depth (left) and momentum (right) over time for the “lake at rest” test case measured in the L^∞ norm.

4.2. Small perturbation over under-resolved bathymetry

To further study the well-balancing property of the method, a small perturbation is added to a fluid at rest. During the experiment, one of the two resulting waves should travel over an exponential bottom topography which is touching the fluid surface only in one point. This numerically challenging test case was proposed by Xing et al. [27]. The domain $[-5, 5]$ is given with a bottom topography $b(x) = 0.5 \exp(-10x^2)$, and the initial condition (see Figure 5) is defined by

$$h(x, 0) = \begin{cases} 0.5 - b(x) + 0.0001 & \text{if } -3 \leq x \leq 2, \\ 0.5 - b(x) & \text{otherwise,} \end{cases} \quad \text{and } u(x, 0) \equiv 0.$$

From the zoomed-in version of the initial data one can see that the tip of the bottom topography becomes singular for coarse grid resolutions. The two waves emerging from the perturbation travel at characteristic speeds $\pm\sqrt{gh}$ to the left and right direction.

In Figure 6 snapshots of the surface elevation at times 0.8, 1.6 and 2.4 are displayed for different resolutions. Due to the singularity of the bottom tip the flow develops some artificial oscillations when the right going wave travels over the tip. This happens especially at the relatively coarse resolution of 250 uniform grid cells. As the resolution becomes finer, the artificial oscillations

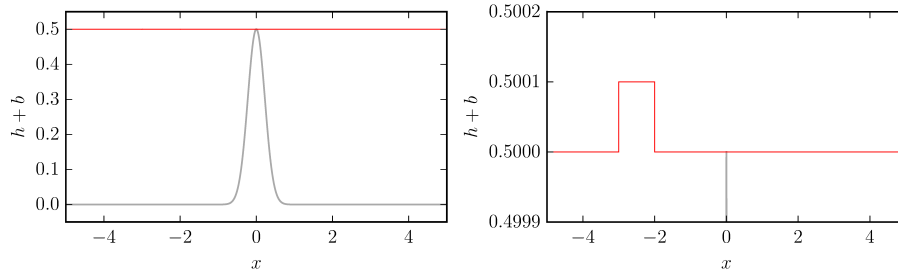


Figure 5: Small perturbation over under-resolved bathymetry. Bottom topography and initial surface elevation. Full view with bottom topography (left), zoomed-in version showing details of initial surface elevation (right).

vanish, which can be seen for the grids with 1250 and 6250 uniform cells. Such oscillatory behavior was also observed by Xing et al. [27] when applying their limiter to the surface elevation H .

4.3. Riemann problems with wet/dry fronts

Riemann problems are usually considered to assess the shock-capturing capabilities of a scheme. Furthermore, they provide an analytical solution to compare with. Here, we setup two different Riemann problems which include dry areas and have been used before to evaluate similar inundation schemes [5, 6, 27] to demonstrate the positivity-preserving capability of the methods. Both problems have a flat bottom ($b \equiv 0$).

The first considered test is a dam break problem with fluid on the left side and a dry area on the right side. The computational domain is $[-300, 300]$ with transparent boundary conditions. The initial conditions are

$$h(x, 0) = \begin{cases} 10 & \text{if } x \leq 0, \\ 0 & \text{otherwise,} \end{cases} \quad \text{and} \quad u(x, 0) \equiv 0 .$$

The analytical solution of this problem is a rarefaction wave and can be found in [5].

For the discretization the domain is divided into 200 uniform intervals. The timestep is 0.05 resulting in a CFL number 0.17. The solution (cell mean values) is displayed at times $t = 4, 8$ and 12 in Figure 7 together with the analytical solution. Besides the fluid depth and the momentum we have also plotted the resulting velocity distribution. The exact solution is well approximated by the simulation results and no instabilities occur. Only a small lag of the wet/dry interface in the numerical solution compared to the exact one can be observed, which can be best seen from the velocity distributions.

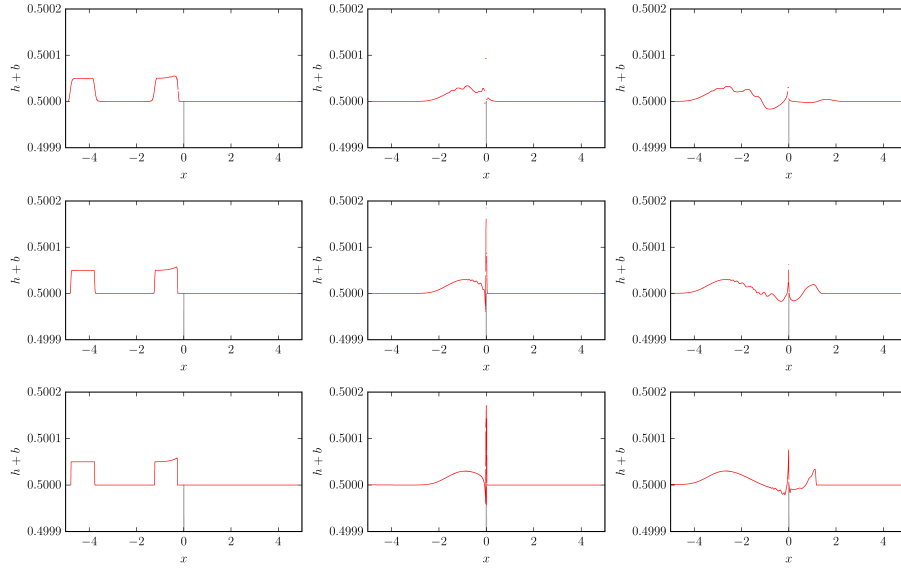


Figure 6: Small perturbation over under-resolved bathymetry. Numerical results of surface elevation at times 0.8, 1.6 and 2.4 (from left to right) for grid resolutions of 250 cells (top), 1250 cells (middle) and 6250 cells (bottom).

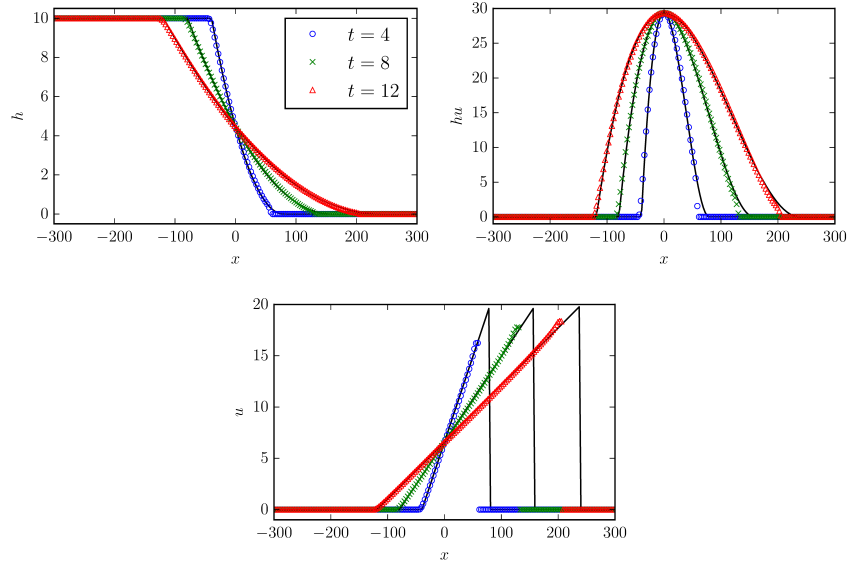


Figure 7: Numerical and exact solution of the dam break problem at times $t = 4, 8$ and 12 . Cell mean values of fluid depth (top left), momentum (top right) and velocity (bottom). The exact solution is given by the black line.

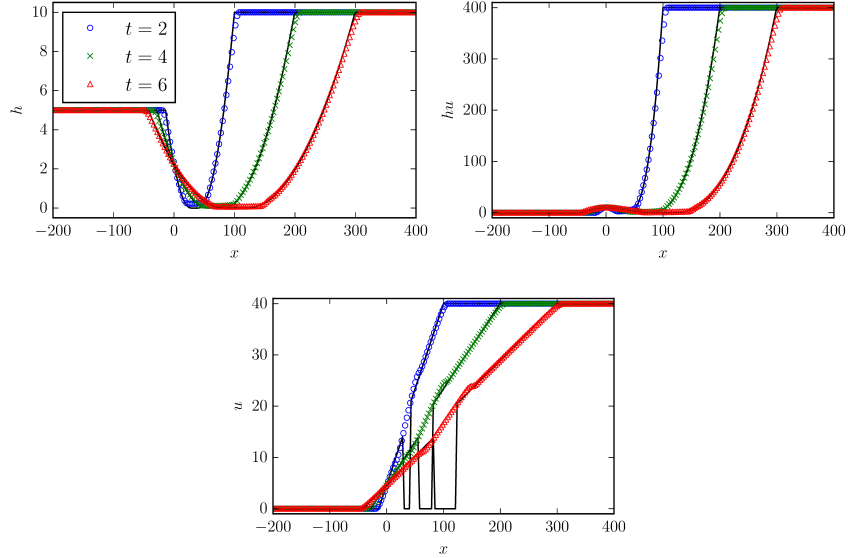


Figure 8: Numerical and exact solution of the Riemann problem with two expansion waves at times $t = 2, 4$ and 6 . Cell mean values of fluid depth (top left), momentum (top right), velocity (bottom). The exact solution is given by the black line.

In the second Riemann problem the domain $[-200, 400]$ is initially wet everywhere with initial conditions

$$h(x, 0) = \begin{cases} 5 & \text{if } x \leq 0, \\ 10 & \text{otherwise,} \end{cases} \quad \text{and} \quad u(x, 0) = \begin{cases} 0 & \text{if } x \leq 0, \\ 40 & \text{otherwise.} \end{cases}$$

Due to the drying condition $\sqrt{gh_l} + u_l < -\sqrt{gh_r} + u_r$, a dry region emerges for $t > 0$, and two expansion waves traveling into opposite directions occur. The analytical solution to this problem can be also found in [5].

The domain is discretized into 200 uniform cells and the timestep is 0.01, which results in a CFL number 0.17. The cell mean values of the simulation are compared to the exact solution in Figure 8 at times $t = 2, 4$ and 6 . Also in this case the analytical solution is well captured. The only problem occurs in the drying area, where the discrete fluid depth does not get below the wet tolerance, resulting in an artificial velocity profile there.

4.4. Oscillatory flow in a parabolic bowl

A numerically challenging test goes back to Thacker [22], where he considers an oscillatory flow in a domain with parabolic bottom topography. Even the analytical solution for the nonlinear shallow water equations is known in this case. This test case has become another standard test problem for inundation

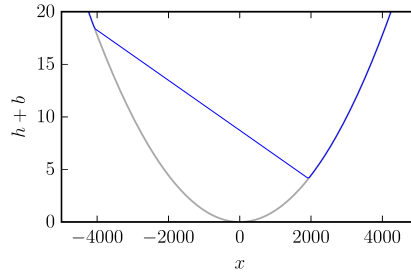


Figure 9: Free surface elevation of an oscillatory flow in a parabolic bowl. Initial condition.

schemes and has been applied to several schemes [e.g. 15, 27]. On the domain $[-5000, 5000]$ the bottom topography is defined by $b(x) = h_0(x/a)^2$, where $a = 3000$ and $h_0 = 10$ define the shape of the parabolic basin. Note that the boundary conditions for the domain are irrelevant since the boundary is in the dry part of the solution. The analytical solution of the water surface is then given by

$$h(x, t) + b(x) = h_0 - \frac{B^2}{4g} (1 + \cos(2\omega t)) - \frac{Bx}{2a} \sqrt{\frac{8h_0}{g}} \cos \omega t,$$

where we set $\omega = \sqrt{2gh_0}/a$ and $B = 5$. Furthermore, the velocity in the wet part is given by

$$u(x, t) \equiv \frac{Baw}{\sqrt{2h_0g}} \sin \omega t.$$

Thus, the solution involves a periodical movement of the wet/dry interface at both sides of the basin. The initial conditions are shown in Figure 9.

The domain is discretized using 200 uniform cells, and a timestep of 1.0 is used, which approximately corresponds to a maximum CFL number of 0.3. We should note that in this case the maximum CFL number with respect to the fluid velocity is about 0.18. This value is achieved in the simulations in the vicinity of the wet/dry interfaces. Therefore, this test case drives the inundation scheme to its stability limits.

The simulation is executed until $t_{\max} = 3000$, when the flow has oscillated a bit more than two periods. The numerical solution compared to the exact one is shown in Figure 10 at times 1000, 2000, 3000. Fluid depth and momentum are well approximated by the DG scheme and indistinguishable from the analytical solution. Only in the velocity field deviations are visible in the vicinity of the wet/dry interface and mostly in case of receding fluid (drying). In these cases a thin film of fluid is left for some time steps and the division of small numbers to compute the velocity leads to these numerical errors. Despite everything, these deviations stay bounded.

These artifacts become smaller if blended limiting is done as described in Section 3.2. This can be seen in Figure 11. Limiting in h clearly improves the

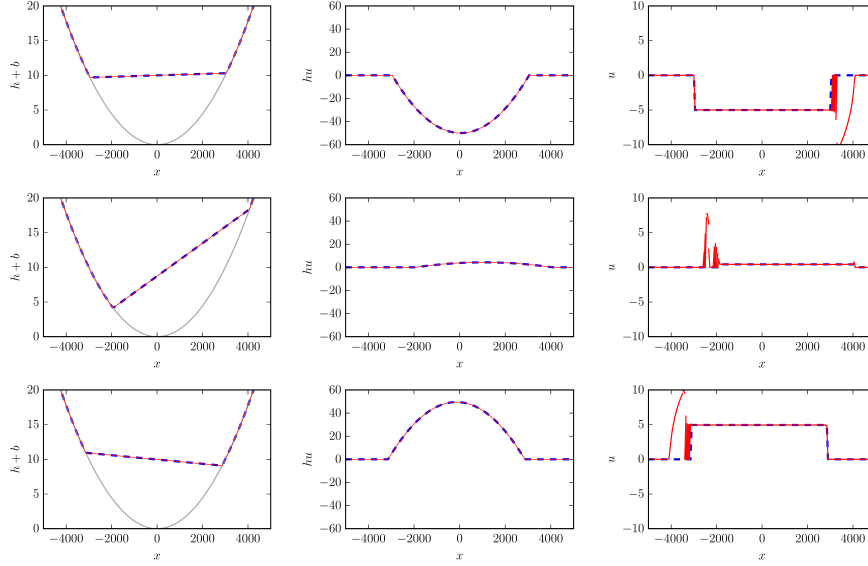


Figure 10: Free surface elevation, momentum and velocity of an oscillatory flow in a parabolic bowl. Numerical (red) and exact solution (blue dashed) at times $t = 1000$, $t = 2000$, $t = 3000$ (from top to bottom). Wet/dry tolerance is set to 10^{-8} . Limiting in surface elevation H .

solution in the vicinity of receding fluid. The discrete solutions for fluid depth and momentum (not shown) are almost indistinguishable from the exact one also in this case.

The test case of an oscillatory flow in a parabolic bowl is also suitable to evaluate the conservation of mass and of total energy $E = \int_{\Omega} hu^2/2 + gh(h/2+b)$ for the numerical method, since there is no flow across the boundary of the domain. In Figure 12 we have plotted the relative mass error and change in total energy with respect to the initial data over time. It can be seen that the mass error is in the range of machine accuracy and there are also only very small fluctuations in total energy.

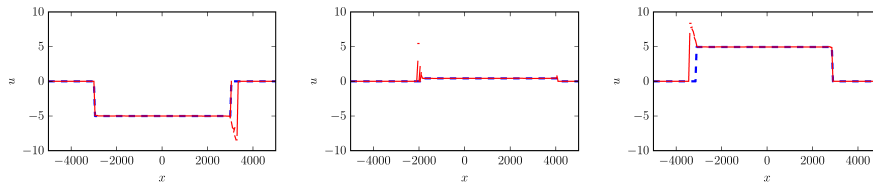


Figure 11: Velocity of an oscillatory flow in a parabolic bowl. Numerical (red) and exact solution (blue dashed) at times $t = 1000$, $t = 2000$, $t = 3000$ (from left to right). Wet/dry tolerance is set to 10^{-8} . Blended limiting.

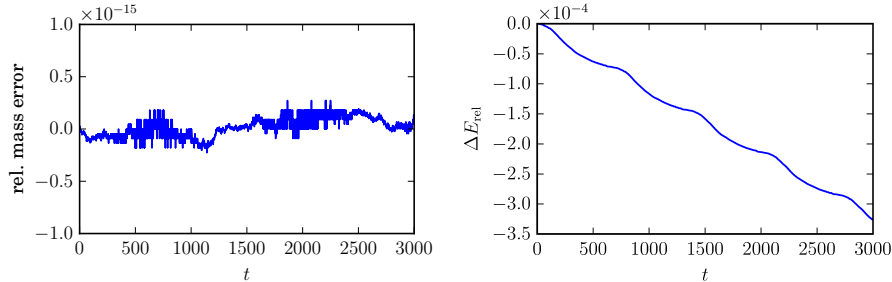


Figure 12: Relative mass error (left) and relative change in total energy of the numerical solution simulating The oscillatory flow in a parabolic bowl.

Another question is the order of convergence of the method. While we cannot expect second order accuracy due to the non-smooth transition between wet and dry regions in the flow variables, the accuracy should be at least around one. For the convergence calculation we have computed the solution up to $t = 1000$ on several grids with cells ranging from 50 to 3200 and fixed CFL number. The experimental convergence rate is calculated by the formula

$$\gamma_c^f := \frac{\log(\|e_c\|/\|e_f\|)}{\log(\Delta x_c/\Delta x_f)}.$$

In this definition, e_c and e_f are the computed error functions of the solution on a coarse and a fine grid (denoted by the number of cells) and Δx_c and Δx_f are the corresponding grid spacings. The results are shown in Figure 13 and Table 1 for the L^2 and L^∞ norms. It can be seen that in the L^2 norm the mean convergence rate is close to 1.5 for both, fluid depth and momentum. In the L^∞ the rates are around 1.0. These low values can be probably explained by the errors arising in the zone of receding water, leading to a small phase error that spoils the maximum norm, but is rather harmless in the two-norm.

We varied the wet tolerance TOL_{wet} for this test case to see how much the stability of the scheme depends on it. Interestingly, we could vary it over a broad range from 10^{-14} to 10^0 and did not even get any stability issues. The parameter merely affected the accuracy of the solution. For $\text{TOL}_{\text{wet}} = 10^0 = 1$, when the parameter is of the order of the solution, large deviations from the exact solution become visible. On the other hand, for a value of 10^{-2} the errors in the velocity field vanish for the most part as can be seen in Figure 14.

4.5. Tsunami runup onto a sloping beach

A more realistic test case is given by the propagation of a tsunami wave onto a uniformly sloping beach. It was originally defined as a benchmark problem in [23]. Besides the slope of the beach the initial surface elevation (Figure 15) and momentum with $(hu)(x, 0) \equiv 0$ is given. The solution is sought on the domain $[-500, 50\,000]$ and the bottom topography is set to $b(x) = 5000 - 0.1x$. At

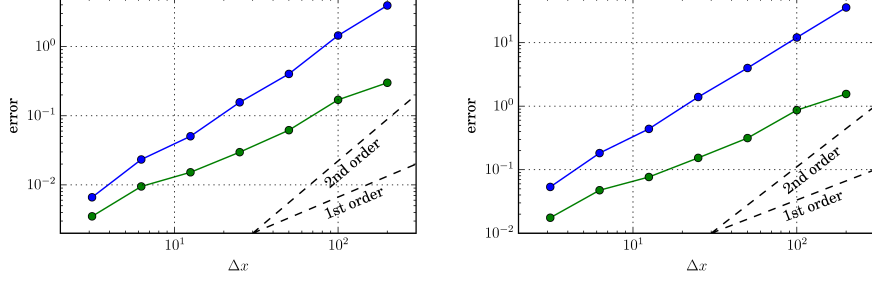


Figure 13: Error of the oscillatory flow in a parabolic bowl test case at $t = 1000$ in the L^2 (blue) and L^∞ (green) norms for different grid sizes. Left: fluid depth, right: momentum.

	$L^2(h)$	$L^2(m)$	$L^\infty(h)$	$L^\infty(m)$
γ_{50}^{100}	1.4437	1.5684	0.8172	0.8462
γ_{100}^{200}	1.8429	1.5948	1.4587	1.4583
γ_{200}^{400}	1.3640	1.5168	1.0561	1.0355
γ_{400}^{800}	1.6303	1.6657	0.9664	1.0002
γ_{800}^{1600}	1.1152	1.2658	0.6804	0.6908
γ_{1600}^{3200}	1.8154	1.7689	1.4353	1.4384
γ_{fitted}	1.5191	1.5503	1.0567	1.0648

Table 1: Convergence rates between different grid levels for the oscillatory flow in a parabolic bowl for fluid depth (h) and momentum (m) in the L^2 and L^∞ norms. Also displayed is the mean convergence rate γ_{fitted} , which is obtained by a least squared fit.

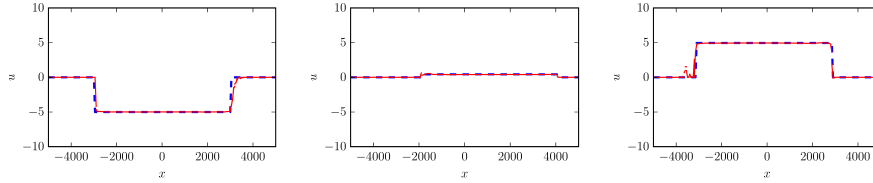


Figure 14: Velocity of an oscillatory flow in a parabolic bowl. Numerical (red) and exact solution (blue dashed) at times $t = 1000$, $t = 2000$, $t = 3000$ (from top to bottom). Wet/dry tolerance is set to 10^{-2} . Limiting in surface elevation H .

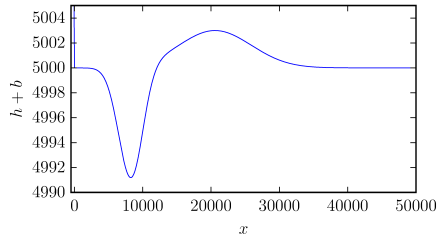


Figure 15: Tsunami runup onto a sloping beach. Initial surface elevation at $t = 0$.

the right boundary of the domain a simple transparent boundary condition is implemented. However, the crucial task is to correctly simulate the inundation process on the interval $[-400, 800]$. The analytical solution at times $t = 160$, 175 and 220 can be derived by the initial-value-problem technique introduced by Carrier et al. [7] and can be found in [23].

In the presented simulation, the domain is discretized into 1010 uniform cells and the timestep is 0.05, which approximately corresponds to a CFL number of 0.22 at the deepest point (right side) of the domain. The results are displayed for the inundation zone in Figure 16, where the fluid depth can also be compared to the analytical solution. At the first observation time $t = 160$ the water recedes, whereas $t = 175$ is the reversal point between drainage and flooding. At the final observation $t = 220$ the coast is still flooded. As in the previous test cases, the analytical fluid depth is well approximated by the discretization. Some spurious velocity deviations can be seen especially in the drying process ($t = 160, 175$), but these are bounded and do not grow over time.

For comparison of the two different limiting procedures, the results for the velocity with blended limiting is shown in Figure 17 (as opposed to limiting in surface elevation in Figure 16). In this case the velocity distributions show slightly more deviations near the wet/dry interface. However, the maximum CFL number with respect to the fluid velocity is much smaller in this test case due to the large fluid depth at the wet end of the domain.

5. Conclusions

In this work a wetting and drying treatment has been proposed for piecewise linear discontinuous Galerkin discretizations of the one-dimensional shallow water equations. It features a velocity based “limiting” of the momentum variable which ensures the schemes’ stability in the vicinity of wet/dry interfaces. The non-destructive limiting of steady states at rest together with a flux modification of semi-dry cells result in a well-balanced method. Several test cases verified the applicability of the scheme to a variety of flow regimes. They show that the scheme is well-balanced, mass conservative and stable for rapid transitions of the edge of the water body. Furthermore, the experimental order of convergence is approximately 1.5 in the L^2 norm and 1 in the maximum norm. The

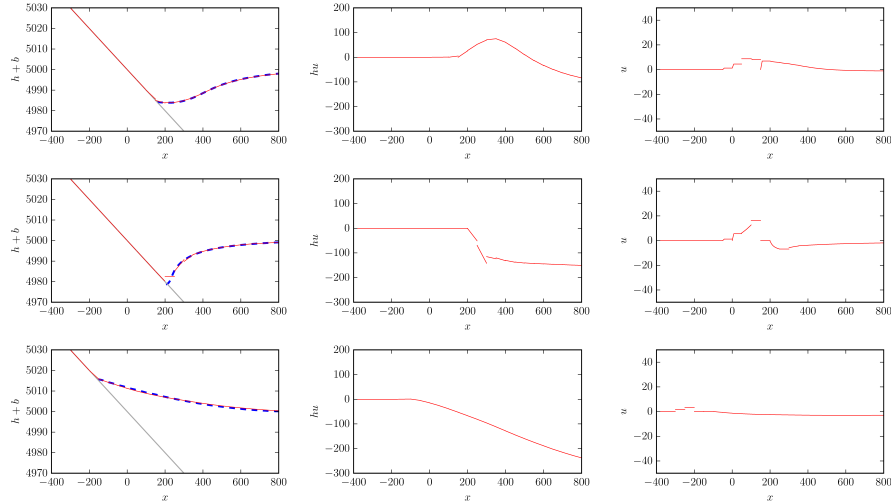


Figure 16: Tsunami runup onto a sloping beach. Computed surface elevation, momentum and velocity from the DG method (red) compared to the exact solution (blue dashed, only for surface elevation) at times $t = 160$ (top), $t = 175$ (middle), $t = 220$ (bottom). Limiting in surface elevation H .

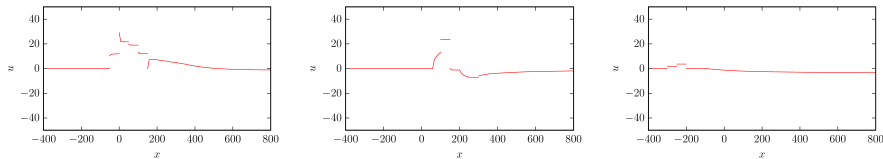


Figure 17: Tsunami runup onto a sloping beach. Computed velocity from the DG method at times $t = 160$ (top), $t = 175$ (middle), $t = 220$ (bottom). Blended limiting.

scheme has only one parameter, which is the wet tolerance, under which a node value is considered to be dry. Computations suggest that the scheme is robust with respect to the particular value of this parameter. Two different limiting strategies were developed in this work: Either by limiting only in the surface elevation $H = h + b$ as it is done in hydrostatic reconstruction methods, or by blending limiting in H and the fluid depth h , the latter resulting in more stable computations in case of rapid wetting and drying. It still has to be investigated, which strategy is better for practical computations.

Beside the major goal of the development of a robust inundation scheme we achieved a simple and straight forward algorithmic structure, which should make it possible to apply the proposed treatment to other DG models. The method is implemented into a second order Runge-Kutta scheme by only a small flux modification and the implementation of the new limiter. The need for positivity,

well-balancedness and stability were clearly addressed by specific components of the algorithm.

The development of limiters for discontinuous Galerkin methods is still under heavy development. The velocity based “limiting” of the momentum resembles the limiting procedure in finite volume methods of other than the primary flow variables (like limiting in primitive or characteristic variables when otherwise working in conservative variables). We are optimistic that the general concept proposed in this work might be transferable to other problems such as DG methods for the solution of invicid compressible flow applications.

Concerning the wetting and drying treatment our target applications are tsunami and storm surge simulations. In this respect the extension of the algorithm to the two-dimensional case is ongoing research. Furthermore, possibilities to extend the proposed concept to higher than linear discontinuous Galerkin elements are investigated.

Acknowledgements. The authors gratefully acknowledge support through the ASCETE (Advanced Simulation of Coupled Earthquake and Tsunami Events) project sponsored by the Volkswagen foundation and through ASTARTE – Assessment, Strategy And Risk Reduction for Tsunamis in Europe. Grant 603839, 7th FP (ENV.2013.6.4-3).

- [1] Audusse, E., Bouchut, F., Bristeau, M.-O., Klein, R., & Perthame, B. (2004). A fast and stable well-balanced scheme with hydrostatic reconstruction for shallow water flows. *SIAM Journal on Scientific Computing*, 25, 2050–2065. doi:10.1137/S1064827503431090.
- [2] Barth, T. J., & Jespersen, D. C. (1989). The design and application of upwind schemes on unstructured meshes. *AIAA Paper*, 89-0366.
- [3] Bates, P. D., & Hervouet, J.-M. (1999). A new method for moving-boundary hydrodynamic problems in shallow water. *Proceedings of the Royal Society of London. Series A: Mathematical, Physical and Engineering Sciences*, 455, 3107–3128. doi:10.1098/rspa.1999.0442.
- [4] Behrens, J. (2010). Numerical methods in support of advanced tsunami early warning. In W. Freeden, M. Z. Nashed, & T. Sonar (Eds.), *Handbook of Geomathematics* chapter 14. (pp. 399–416). Springer. doi:10.1007/978-3-642-01546-5_14.
- [5] Bokhove, O. (2005). Flooding and drying in discontinuous Galerkin finite-element discretizations of shallow-water equations. part 1: One dimension. *Journal of Scientific Computing*, 22–23, 47–82. doi:10.1007/s10915-004-4136-6.
- [6] Bunya, S., Kubatko, E. J., Westerink, J. J., & Dawson, C. (2009). A wetting and drying treatment for the Runge-Kutta discontinuous Galerkin solution to the shallow water equations. *Comput. Methods Appl. Mech. Engrg.*, 198, 1548–1562. doi:10.1016/j.cma.2009.01.008.

- [7] Carrier, G. F., Wu, T. T., & Yeh, H. (2003). Tsunami run-up and draw-down on a plane beach. *Journal of Fluid Mechanics*, 475, 79–99. doi:10.1017/S0022112002002653.
- [8] Einfeldt, B. (1988). On Godunov-type methods for gas dynamics. *SIAM Journal on Numerical Analysis*, 25, 294–318. doi:10.1137/0725021.
- [9] Ern, A., Piperno, S., & Djadel, K. (2008). A well-balanced Runge-Kutta discontinuous Galerkin method for the shallow-water equations with flooding and drying. *International Journal for Numerical Methods in Fluids*, 58, 1–25. doi:10.1002/flid.1674.
- [10] Giraldo, F. X., & Warburton, T. (2008). A high-order triangular discontinuous Galerkin oceanic shallow water model. *International Journal for Numerical Methods in Fluids*, 56, 899–925. doi:10.1002/flid.1562.
- [11] Gottlieb, S., Shu, C.-W., & Tadmor, E. (2001). Strong stability-preserving high-order time discretization methods. *SIAM Review*, 43, 89–112. doi:10.1137/S003614450036757X.
- [12] Gourgue, O., Comblen, R., Lambrechts, J., Kärnä, T., Legat, V., & Deleersnijder, E. (2009). A flux-limiting wetting–drying method for finite-element shallow-water models, with application to the Scheldt Estuary. *Advances in Water Resources*, 32, 1726–1739. doi:10.1016/j.advwatres.2009.09.005.
- [13] Hesthaven, J. S., & Warburton, T. (2008). *Nodal discontinuous Galerkin methods: algorithms, analysis, and applications*. Springer.
- [14] Hu, C., & Shu, C.-W. (1999). Weighted essentially non-oscillatory schemes on triangular meshes. *Journal of Computational Physics*, 150, 97–127. doi:10.1006/jcph.1998.6165.
- [15] Kesserwani, G., & Liang, Q. (2010). Well-balanced RKDG2 solutions to the shallow water equations over irregular domains with wetting and drying. *Computers & Fluids*, 39, 2040–2050. doi:10.1016/j.compfluid.2010.07.008.
- [16] Liang, Q., & Marche, F. (2009). Numerical resolution of well-balanced shallow water equations with complex source terms. *Advances in Water Resources*, 32, 873–884. doi:10.1016/j.advwatres.2009.02.010.
- [17] Nielsen, C., & Apelt, C. (2003). Parameters affecting the performance of wetting and drying in a two-dimensional finite element long wave hydrodynamic model. *Journal of Hydraulic Engineering*, 129, 628–636. doi:10.1061/(ASCE)0733-9429(2003)129:8(628).
- [18] Popinet, S. (2012). Adaptive modelling of long-distance wave propagation and fine-scale flooding during the Tohoku tsunami. *Natural Hazards and Earth System Science*, 12, 1213–1227. doi:10.5194/nhess-12-1213-2012.

- [19] Shu, C.-W., & Osher, S. (1988). Efficient implementation of essentially non-oscillatory shock-capturing schemes. *Journal of Computational Physics*, 77, 439–471. doi:10.1016/0021-9991(88)90177-5.
- [20] Sonar, T. (1997). On the construction of essentially non-oscillatory finite volume approximations to hyperbolic conservation laws on general triangulations: polynomial recovery, accuracy and stencil selection. *Computer Methods in Applied Mechanics and Engineering*, 140, 157–181. doi:10.1016/S0045-7825(96)01060-2.
- [21] Synolakis, C. E., & Bernard, E. N. (2006). Tsunami science before and beyond Boxing Day 2004. *Phil. Trans. R. Soc. A*, 364, 2231–2265. doi:10.1098/rsta.2006.1824.
- [22] Thacker, W. C. (1981). Some exact solutions to the nonlinear shallow-water wave equations. *Journal of Fluid Mechanics*, 107, 499–508. doi:10.1017/S0022112081001882.
- [23] The Third International Workshop on Long-Wave Runup Models (2004). Benchmark problem #1: Tsunami runup onto a plane beach. http://isec.nacse.org/workshop/2004_cornell/bmark1.html.
- [24] Toro, E. F. (2009). *Riemann Solvers and Numerical Methods for Fluid Dynamics: A Practical Introduction*. (3rd ed.). Springer.
- [25] Xing, Y., & Shu, C.-W. (2006). A new approach of high order well-balanced finite volume weno schemes and discontinuous Galerkin methods for a class of hyperbolic systems with source terms. *Communications in Computational Physics*, 1, 100–134.
- [26] Xing, Y., & Shu, C.-W. (2011). High-order finite volume WENO schemes for the shallow water equations with dry states. *Advances in Water Resources*, 34, 1026–1038. doi:10.1016/j.advwatres.2011.05.008.
- [27] Xing, Y., Zhang, X., & Shu, C.-W. (2010). Positivity-preserving high order well-balanced discontinuous Galerkin methods for the shallow water equations. *Advances in Water Resources*, 33, 1476–1493. doi:10.1016/j.advwatres.2010.08.005.